Chinese Journal of
POLYMER SCIENCE

ARTICLE

https://doi.org/10.1007/s10118-020-2372-3
Chinese J. Polym. Sci. **2020**, *38*, 704–714

Antibacterial and pH-responsive Quaternized Hydroxypropyl Cellulose-*g*-Poly(THF-*co*-epichlorohydrin) Graft Copolymer: Synthesis, Characterization and Properties

Jin-Rui Deng, Cong-Lei Zhao, and Yi-Xian Wu*

State Key Laboratory of Chemical Resource Engineering, Beijing Advanced Innovation Center for Soft Matter Science and Engineering, Beijing Laboratory of Biomedical Materials, Beijing University of Chemical Technology, Beijing 100029, China

Electronic Supplementary Information

Abstract The novel quaternized hydroxypropyl cellulose-*g*-poly(THF-*co*-epichlorohydrin) graft copolymers, HPC-*g*-QCP(THF-*co*-ECH), have been successfully synthesized to combine the properties from hydrophilic hard HPC biomacromolecular backbone and hydrophobic flexible polyether branches. Firstly, the P(THF-*co*-ECH) living chains were synthesized by cationic ring-opening copolymerization of THF with ECH. Secondly, P(THF-*co*-ECH) living chains were grafted onto HPC backbone by reaction with —OH groups along HPC to produce HPC-*g*-P(THF-*co*-ECH) graft copolymers. Thirdly, the mentioned graft copolymers were quaternized by reaction with ternary amine to generate functionalized HPC-*g*-QCP(THF-*co*-ECH). The HPC-*g*-QCP(THF-*co*-ECH) graft copolymers exhibited good antibacterial ability against *S. aureus* or *E. coli* bacteria. The ibuprofen (IBU)-loaded microparticles of HPC-*g*-(QC)P(THF-*co*-ECH) graft copolymers were prepared by electrospraying. The *in vitro* pH-responsive drug-release behavior of IBU reached up to 75% of drug-loaded at pH = 7.4. This quaternized graft copolymer was beneficial to solving the problems of a burst effect and fast release of HPC as drug carriers.

Keywords Living cationic ring-opening copolymerization; Hydroxypropyl cellulose-graft-polyether; Antibacterial ability; pH-responsive drug-release

Citation: Deng, J. R.; Zhao, C. L.; Wu, Y. X. Antibacterial and pH-responsive quaternized hydroxypropyl cellulose-*g*-poly(THF-*co*-epichlorohydrin) graft copolymer: synthesis, characterization and properties. *Chinese J. Polym. Sci.* **2020**, *38*, 704–714.

INTRODUCTION

Aliphatic polyethers are important polymers for an immense variety of applications. Polyether-based materials with unique C—O—C bond backbone have gathered particular focus because of their typical properties of high flexibility and hydrophilicity. Polyether can be generated by ring-opening polymerization (ROP) of the commercial three- to five-membered cyclic ethers.[1] Additionally, other classes of epoxide monomers that contain reactive functional groups, such as epichlorohydrine (ECH), glycidyl ether, and glycidyl amine, can be used as comonomers to introduce versatile possibilities and post-modifications on account of the presence of new structural units in the polyether chains. In particular, poly(tetrahydrofuran) (PTHF) can be generated by cationic ROP (CROP) of THF, which is an extremely peerless material due to its nonpolarity, excepted to aforementioned properties.[2–4] What is more, good solubility, low melting point (easy to handling), and high hydrolytic stability endow PTHF-based materials with fully wide applications for polyurethane production,[5,6] adhesives or sealants.[7,8] PTHF has also been widely used in biomedical applications because of its good biocompatibility, hydrophobicity, flexibility, and biosafety.[9]

The past decades have experienced an explosive growth in study of natural polysaccharides which are available from renewable resources. Polysaccharides represent the ideal biocompatible materials for their biocompatibility, biosafety, and biodegradability. Polysaccharides have been widely used in the biomedical fields of drug delivery system[10] and tissue engineering scaffold.[11] Cellulose is the amplest biopolymer with about annual production of 7.5×10^{10} tons per year.[12] The insolubility of cellulose in common solvents, caused by the intramolecular and intermolecular H-bonding networks, limits its applications. Many chemical modifications for hydroxyl groups at cellulose have been used to construct new cellulosic materials. Hydroxypropyl cellulose (HPC) derivated from cellulose with some hydroxyl groups hydroxypropylation has drawn much attention for its good solubility and safety, which has been widely used in the fields of food and drug.[13–16]

Several grafting approaches have been developed to chemically modify the cellulose and cellulosic derivatives by grafting reaction of other synthetic polymer chains, such as "grafting onto" and "grafting from".[17–19] For the examples of

* Corresponding author, E-mail: wuyx@mail.buct.edu.cn

Received October 9, 2019; Accepted November 14, 2019; Published online January 6, 2020

"grafting onto" method, there are cellulose-*g*-poly(methyl methacrylate),[20] cellulose nanocrystal-*g*-poly(lactic acid)-hydrocarbon chain,[21] carboxyethyl cellulose-*g*-dithiodipropionate dihydrazide, and dibenzaldehyde-terminated poly(ethylene glycol).[22] The examples of synthetic polymer chains of cellulose graft copolymers by "grafting from" approach include poly(*p*-dioxanone),[23] poly(acrylic acid) or polyacrylamide,[24–27] polyethyleneamidoamine,[28] polyethyleneimine,[29,30] polyamidoxime,[31] poly(D-lactide),[32] poly(2-(methacryloyloxy) ethyl phosphorylcholine),[33] polystyrene,[34] poly(ε-caprolactone)-*b*-poly(*N*,*N*-dimethylaminoethylmethacrylate),[35] and polyacrylonitrile.[36] However, there has been no report on polyether-grafted HPC materials.

In order to endow traditional HPC materials with multifunctional properties such as antibacterial property and pH-response as drug carriers, herein we synthesized the quaternized hydroxypropyl cellulose-*g*-poly(THF-*co*-ECH) graft copolymers *via* combining living CROP of THF with ECH, controlled termination of living P(THF-*co*-ECH) chains with —OH groups in structural units on HPC hard backbone and quaternization. We anticipate that the quaternized graft copolymer of HPC-*g*-QCP(THF-*co*-ECH) could take advantages of renewable hydrophilic hard HPC materials and biocompatible hydrophobic flexible polyether chains. The graft copolymers of HPC-*g*-QCP(THF-*co*-ECH) showed good antibacterial ability against *S. aureus* or *E. coli* bacteria and solved the problems of a burst effect and fast release of HPC as drug carriers. The crystalline morphology and surface tension of HPC-*g*-P(THF-*co*-ECH) graft copolymers were also investigated. These new polyether-grafted cellulosic materials would improve the comprehensive properties of HPC-based materials for antibacterial and drug delivery systems.

EXPERIMENTAL

Materials and Reagents

Tetrahydrofuran (THF, Beijing Chemical Company) was refluxed with sodium wire using benzophenone as an indicator until the solution showed blue color before use. Epichlorohydrin (ECH, Beijing Chemical Company) and methyl triflate (MeOTf, J&K, 98%) were treated with 4Å molecular sieve. Dichloromethane (DCM, Beijing Chemical Company) was refluxed with calcium hydride before use. Hydroxypropyl cellulose (HPC, ~100 kg·mol^{-1}, degree of substitution (DS) (hydroxypropyl, HP) and molar substitution (MS) were determined by ^{1}H-NMR) was dried at 70 °C in a vacuum oven before use. Ethanol (Beijing Chemical Company) and *n*-hexane (Beijing Chemical Company) were used without further purification. Regenerated cellulose membranes (MWCO 50000) were supplied by Shanghai Yuanye Bio-Technology Co., Ltd.

Synthesis of Living P(THF-*co*-ECH) Chains *via* Living CROP

Living P(THF-*co*-ECH) chains were prepared by living CROP of ECH and THF with various feed ratios. For example, ECH (3.701 g, 0.04 mol, 92.52 g·mol^{-1}), THF (25.942 g, 0.36 mol, 72.06 g·mol^{-1}), and 30 mL of fresh DCM were added into a clean pre-baked glass tube with a magnetic stir bar under N_2 atmosphere at 25 °C. Then, methyl triflate (MeOTf) (26 μL) was added. P(THF-*co*-ECH) living chains were obtained in the reaction systems after 24 h. And at the same time, a part solution was taken out from the reaction systems and then was quenched with water for determining the M_n, MWD and chemical structure of the end groups.

Synthesis of HPC-*g*-P(THF-*co*-ECH) Graft Copolymer *via* Controlled Termination

HPC (0.5 g, 1.20 mmol anhydroglucose unit (AGU)) was dissolved in 20 mL of anhydrous DCM under stirring for 3 h at 25 °C. And then, the above HPC solution in DCM was added into the living copolymer solution under stirring for another 5 h to complete the reaction. Then, the reaction mixture solution was dialyzed in THF through regenerated cellulose membranes (MWCO 50000) for 7 days to remove the possible unreacted P(THF-*co*-ECH) copolymer chains. Finally, the graft polymer solution was dropped into a lot of *n*-hexane to precipitate the possible as-formed HPC-*g*-P(THF-*co*-ECH) graft copolymers. The final weight of HPC-*g*-P(THF-*co*-ECH) graft copolymers was determined after drying in the vacuum oven.

Quaternization of Branches in HPC-*g*-P(THF-*co*-ECH) Graft Copolymer

The partially quaternized HPC-g_{24}-QCP(THF_{133}-*co*-ECH_{11}) graft copolymers were prepared in 5 mL of THF containing 0.1 g of HPC-g_{24}-P(THF_{133}-*co*-ECH_{11}) with 0.003 mmol of P(THF_{133}-*co*-ECH_{11}) branches and 1.0 mL of triethylamine ($N(C_2H_5)_3$) or trioctylamine ($N(C_8H_{17})_3$) at 60 °C for 24 h. The HPC-*g*-QCP(THF-*co*-ECH) copolymers were precipitated in a lot of *n*-hexane and dried under vacuum. The two resulted quaternization products were denoted as HPC-*g*-QC_2P(THF-*co*-ECH) and HPC-*g*-QC_8P(THF-*co*-ECH), respectively.

Characterization

The detailed procedures of characterization are described in the electronic supplementary information (ESI).

RESULTS AND DISCUSSION

The synthetic strategy for the quaternized hydroxypropyl cellulose-*g*-poly(THF-*co*-epichlorohydrin) graft copolymers, HPC-*g*-QCP(THF-*co*-ECH), to combine the properties from hydrophilic hard HPC biomacromolecule backbone, hydrophobic flexible polyether branches and functional groups, is shown in Scheme 1. The synthetic routes include three steps: (1) synthesis of P(THF-*co*-ECH) living chains by CROP of THF with ECH; (2) synthesis of HPC-*g*-P(THF-*co*-ECH) graft copolymer by grafting P(THF-*co*-ECH) living chains onto HPC backbone by nucleophile substitution reaction with the —OH side groups along HPC macromolecules; (3) quaternization of HPC-*g*-P(THF-*co*-ECH) graft copolymer through Menshutkin reaction.

Living CROP of THF and ECH

The schematic illustration for living P(THF-*co*-ECH) chains *via* living CROP is given in Scheme 1(a). A series of P(THF-*co*-ECH) copolymer living chains with various feed ratios of THF to ECH were successfully prepared in the present work according to our previous works on living CROP of THF.[37–40] ECH with a chlorine atom pendant was selected as a comonomer for synthesis of copolyether with THF. The copolymerization of THF and ECH with various feed ratios was carried out using MeOTf as an efficient and quantitative initiator at 25 °C.

In order to obtain and characterize the M_n, MWD and end

https://doi.org/10.1007/s10118-020-2372-3

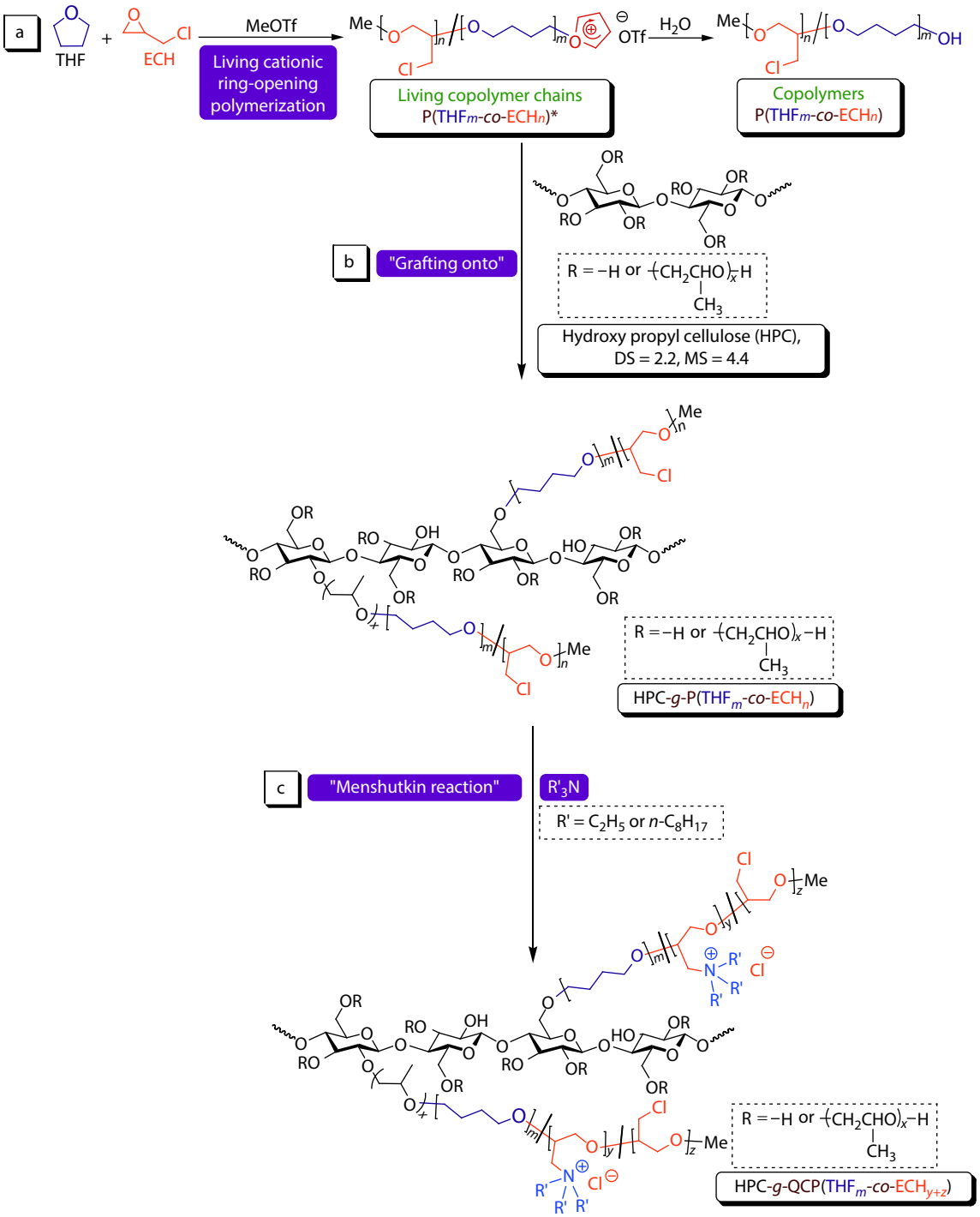

Scheme 1 Schematic illustration for quaternized hydroxypropyl cellulose-*g*-poly(THF-*co*-epichlorohydrin) graft copolymers.

functional groups in the resulting PTHF homopolymer and P(THF-*co*-ECH) random copolymers from living P(THF-*co*-ECH) chains, water containing hydroxyl group was selected as a model molecule to terminate the above living polymers. The resultant PTHF homopolymer and P(THF-*co*-ECH) copolymers with various ECH fractions were characterized by FTIR and the corresponding FTIR spectra are presented in Fig. S3 (in ESI). The bands at about 2800 and 1100 cm^{-1} are attributed to C—H and C—O bond stretching, respectively. Especially, the absorbance in the fingerprint region at 750 cm^{-1} represents the C—Cl bond stretching in ECH unit in the copolymers. The intensity of the band at 750 cm^{-1} increased with the increase in ECH molar fraction in monomer feeds (Fig. S3 in ESI). The FTIR spectra indicate the successful synthesis of P(THF-*co*-ECH) copolymers with various ECH contents.

The resulting P(THF-*co*-ECH) random copolymers were further characterized by ^{1}H-NMR spectroscopy to determine their compositions. The representative ^{1}H-NMR spectra of

https://doi.org/10.1007/s10118-020-2372-3

P(THF_{201}-*co*-ECH_{15}) and P(THF_{104}-*co*-ECH_{26}) copolymers are shown in Fig. S4 (in ESI). The ECH contents in the P(THF-*co*-ECH) copolymers were determined to be in a range from 6.9 mol% to 19.7 mol%. The resonance signals of polyether belonging to the THF units appear at 1.50–1.70 ppm (Fig. S4b in ESI) and 3.31–3.44 ppm (Fig. S4a in ESI). The signals of polyether belonging to the ECH units appear in the range of 3.42–4.0 ppm (Figs. S4c, S4d, and S4e in ESI). The signal at around 2.0 ppm is assigned to proton of hydroxy group. What is more, the signal at 3.30 ppm is attributed to the methyl head-group (from initiator MeOTf). The aforementioned ^{1}H-NMR analysis together with the FTIR characterization confirms the successful synthesis of P(THF-*co*-ECH) copolymers and the quantitative termination of living P(THF-*co*-ECH) chains by H_2O molecules.

An overview of the curves collected from the gel permeation chromatography analyses of PTHF homopolymer and P(THF-*co*-ECH) random copolymers with various ECH incorporation ratios from 6.9 mol% to 19.7 mol% is given in Fig. 1. The detail information on MWD (M_w/M_n) of all samples is also presented in Fig. 1. It is well documented that M_n ranges from 8900 g·mol^{-1} to 5.38 × 10^4 g·mol^{-1} with unimodal molecular weight distribution.

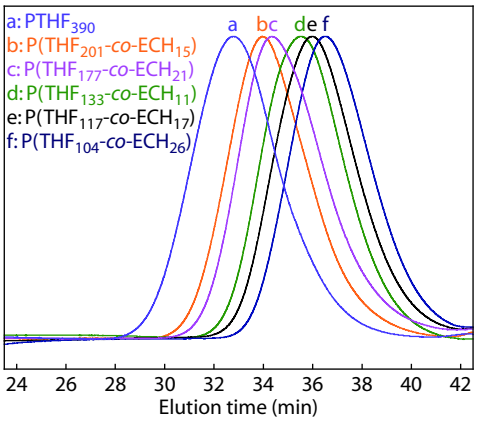

Fig. 1 Representative GPC traces (in THF, PS standards) of PTHF homopolymer and P(THF-*co*-ECH) random copolymers with various ECH incorporation ratios (from 6.9 mol% to 19.7 mol%). (a) feed ratio of THF/ECH = 100/0 (mol/mol), $PTHF_{390}$, M_n = 5.38 × 10^4 g·mol^{-1}, M_w/M_n = 1.99; (b) feed ratio of THF/ECH = 95/5 (mol/mol), P(THF_{201}-*co*-ECH_{15}), M_n = 2.66 × 10^4 g·mol^{-1}, M_w/M_n = 1.89; (c) feed ratio of THF/ECH = 90/10 (mol/mol), P(THF_{177}-*co*-ECH_{21}), M_n = 2.10 × 10^4 g·mol^{-1}, M_w/M_n = 1.83; (d) feed ratio of THF/ECH = 80/20 (mol/mol), P(THF_{133}-*co*-ECH_{11}), M_n = 1.47 × 10^4 g·mol^{-1}, M_w/M_n = 1.80; (e) feed ratio of THF/ECH = 70/30 (mol/mol), P(THF_{117}-*co*-ECH_{17}), M_n = 1.18 × 10^4 g·mol^{-1}, M_w/M_n = 1.78; (f) feed ratio of THF/ECH = 60/40 (mol/mol), P(THF_{104}-*co*-ECH_{26}), M_n = 8900 g·mol^{-1}, M_w/M_n = 1.79. Conditions: polymerization in DCM using methyl trifluoromethanesulfonate (MeOTf) as an initiator under nitrogen at 25 °C for 24 h.

The thermal properties of P(THF-*co*-ECH) random copolymers have been studied by DSC. The increased ECH content in the THF-enriched segments may have an impact on the thermal properties of the copolymers. Figs. 2(A) and 2(B) present the DSC results of P(THF_{201}-*co*-ECH_{15}), P(THF_{177}-*co*-ECH_{21}) copolymers around M_n of 2.00 × 10^4 g·mol^{-1} and P(THF_{133}-*co*-ECH_{11}), P(THF_{117}-*co*-ECH_{17}), P(THF_{104}-*co*-ECH_{26}) copolymers with about M_n of around 1.00 × 10^4 g·mol^{-1}, respectively. These curves are typical of long chain aliphatic polyethers with a high tendency to crystallize into good and stable crystals. It can be seen from Fig. 2 that the crystallization temperature (T_c) decreased notably from −8 °C (6.9 mol% ECH) to −29 °C (19.7 mol% ECH) while T_c of $PTHF_{390}$ (M_n = 5.38 × 10^4 g·mol^{-1}) was −4 °C with increasing the amount of ECH in the copolymers. A few of ECH units embedded into the segments of THF units resulted in a decrease in the T_c of THF units, which visibly disturbed the crystalline structure of PTHF segments. The melting points (T_m) and glass transition temperatures (T_g) of P(THF-*co*-ECH) random copolymers with ECH fractions from 6.9% to 19.7% are also given in Fig. 2. The same trend for T_c and for T_m can be seen for P(THF-*co*-ECH) random copolymers, in which T_m decreased from 24 °C to 16 °C with increasing ECH content from 6.9 mol% to 19.7 mol%. The single melting endotherm can be observed for P(THF-*co*-ECH) random copolymers with 6.9 mol% to 10.6 mol% ECH. It indicates that the resultant crystals are considered to be good and stable; accordingly, they melt directly without undergoing reorganization and recrystallization. It is worth mentioning that both the P(THF_{117}-*co*-ECH_{17}) (12.4% ECH) and P(THF_{104}-*co*-ECH_{26}) (19.7% ECH) random copoly-

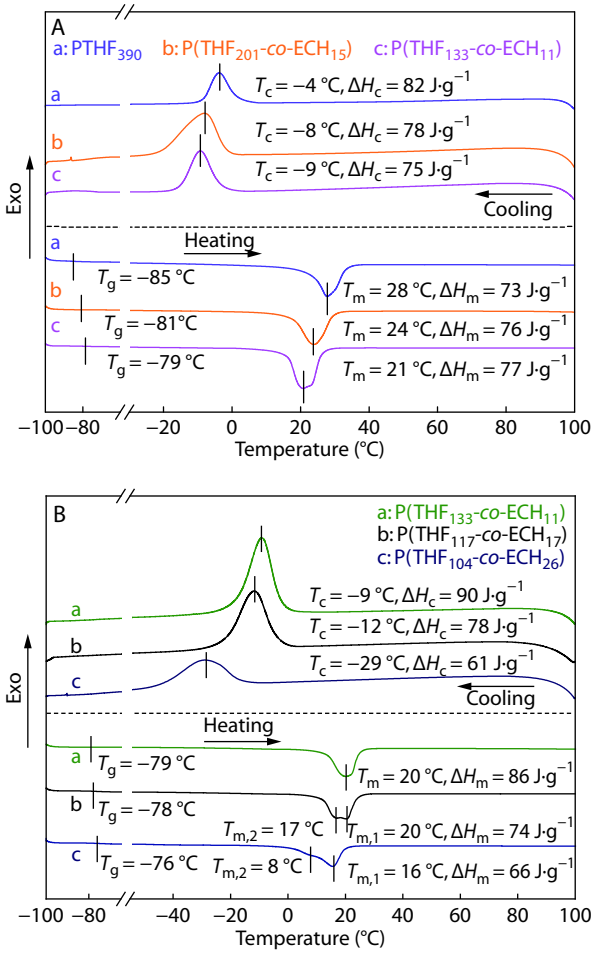

Fig. 2 DSC curves of several P(THF-*co*-ECH) copolymers with various ECH incorporation ratios (from 6.9 mol% to 19.7 mol%), heating and cooling cycle at 20 °C·min^{-1}.

https://doi.org/10.1007/s10118-020-2372-3

mers show two peaks in T_m, which is attributed to the low crystallization rate and low flexibility of the polymer with short —(CH_2)— sequences. Two melting transitions ($T_{m,1}$ = 16 °C, $T_{m,2}$ = 8 °C) to crystalline packing could be determined for P(THF_{104}-*co*-ECH_{26}) copolymer (19.7% ECH).

The bulky pendant groups of chlorine atoms in the random copolymers seem to impede the crystallization process. The T_g of the $PTHF_{390}$ homopolymer was determined to be –85 °C. On the other hand, all the T_gs of P(THF-*co*-ECH) copolymers with various ECH incorporation ratios are higher than that of $PTHF_{390}$, indicating several ECH units embedded into copolymer chains inhibit the movement of the PTHF segments in random copolymers. These results demonstrate that P(THF-*co*-ECH) random copolymer would be a good candidate for soft branches in the desired HPC-*g*-P(THF-*co*-ECH) graft copolymers.

Synthesis and Characterization of HPC-*g*-P(THF-*co*-ECH) *via* Nucleophile Substitution of Living P(THF-*co*-ECH) Chains with —OH Groups along HPC Main Chains

The HPC-*g*-P(THF-*co*-ECH) graft copolymers were synthesized *via* nucleophile substitution of living P(THF-*co*-ECH) chains with the —OH groups along HPC chains (Scheme 1b).

The functional terminated living P(THF-*co*-ECH) chains could be prepared by adding the living P(THF-*co*-ECH) chain solution into the HPC solution in DCM at 25 °C. The average number of P(THF-*co*-ECH) branches (G_N) grafted onto HPC backbone per 1000 anhydroglucose units of the HPC was 23, 24, 24, 27 and 28 by changing the molar ratios of living chains (from 0.027 mmol to 0.033 mmol) to HPC. The corresponding resultant graft copolymers are expressed as HPC-g_{23}-P(THF_{201}-*co*-ECH_{15}), HPC-g_{24}-P(THF_{177}-*co*-ECH_{21}), HPC-g_{24}-P(THF_{133}-*co*-ECH_{11}), HPC-g_{27}-P(THF_{117}-*co*-ECH_{17}) and HPC-g_{28}-P(THF_{104}-*co*-ECH_{26}), respectively.

The changes in chemical structure of HPC biomacromolecules after graft modification were characterized by FTIR and the representative FTIR spectra of HPC and HPC-g_{24}-P(THF_{133}-*co*-ECH_{11}) graft copolymer are showed in Fig. S5 (in ESI). Compared to HPC, the band at about 3446 cm^{-1} for the stretching vibrations of the OH side groups in HPC weakened after the graft modification. And the intensity of bands from 2980 cm^{-1} to 2850 cm^{-1} assigned to C—H vibration and band at about 1100 cm^{-1} belonging to C—O bond increased after the graft modification.

The representative ^{1}H-NMR spectra of HPC and the resulting graft copolymers with various grafting density and branch length in $CDCl_3$ are presented in Fig. 3. The signal at δ = 1.12 ppm is responsible for the CH_3 protons of propylene oxide groups (c). The signals at δ = 1.61 ppm and δ = 3.34 ppm are associated with the CH_2 protons (b) and O—CH_2 protons (a) of THF units in the branches. The signals with the chemical shifts from 2.9 ppm to 4.3 ppm belong to the inner CH and CH_2 protons on AGU and propylene groups. The chemical shift of the CH_2 protons in ECH moieties in the branches is totally overlapped with AGU signal of HPC, leading to difficulty in measuring the degree of substitution of —OH groups substituted per AGU of HPC backbone.

The effects of M_n of branches and G_N on the crystallization behavior of HPC-*g*-P(THF-*co*-ECH) graft copolymers were further investigated by POM. The POM images of HPC and HPC-*g*-P(THF-*co*-ECH) graft copolymers with various compositions are given in Fig. 4. Fig. 4(a) depicts that the crystalline morphology of HPC has a grain-like structure at 20 °C. The crystalline morphology of HPC-*g*-P(THF-*co*-ECH) graft copolymers generally changed from grain-like structure to band-like structure with increasing M_n of branches and decreasing G_N. It is likely due to the reason that the less ordered grain-like crystalline morphology is mainly dependent on the HPC main chains for the HPC-*g*-P(THF-*co*-ECH) graft copolymers with short branch length. On the other hand, the band-like structure crystalline morphology is mainly dependent on the polyether branches in the HPC-*g*-P(THF-*co*-ECH) graft copolymers with long branch length. The nucleation density of each sample became smaller and the size of band-like structure crystalline morphology became larger prior to their impinging against each other with increased branch length, which might be resulted from the twisting of long chain aliphatic polyether branches.

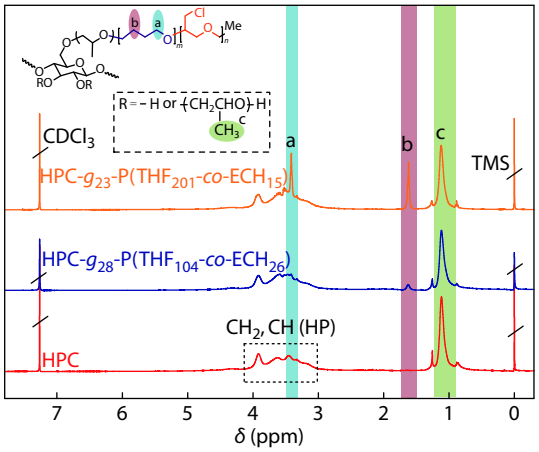

Fig. 3 ^{1}H-NMR spectra of HPC and HPC-*g*-P(THF-*co*-ECH) graft copolymers with different compositions.

Water contact angle (WCA) on polymer film surface reflects the change of functional groups or micro/nano structure. WCA measurement on HPC and HPC-*g*-P(THF-*co*-ECH) graft copolymer films is given in Fig. 5(a). The contact angle of water droplets on HPC film was 55.6° and increased after graft modification. The contact angles on HPC-*g*-P(THF-*co*-ECH) graft copolymer films were ranging from 58.7° to 82.4° under the same conditions, reflecting that the materials show the improvement of hydrophobicity with low surface tension.

Functionalization and Characterization of Quaternized HPC-*g*-QCP(THF-*co*-ECH) Graft Copolymers, and Their Applications for Drug Carriers and Antibacterial Materials

Scheme 1(c) illustrates the synthetic strategy for preparing HPC-*g*-QCP(THF-*co*-ECH) graft copolymers *via* Menshutkin reaction. The chlorine atom functional pendants in ECH units were further reacted with tertiary amines to form quaternary ammonium cations, leading to the attachment of new functional groups.

As shown in Fig. S6 (FTIR spectra in ESI), the new band at

https://doi.org/10.1007/s10118-020-2372-3

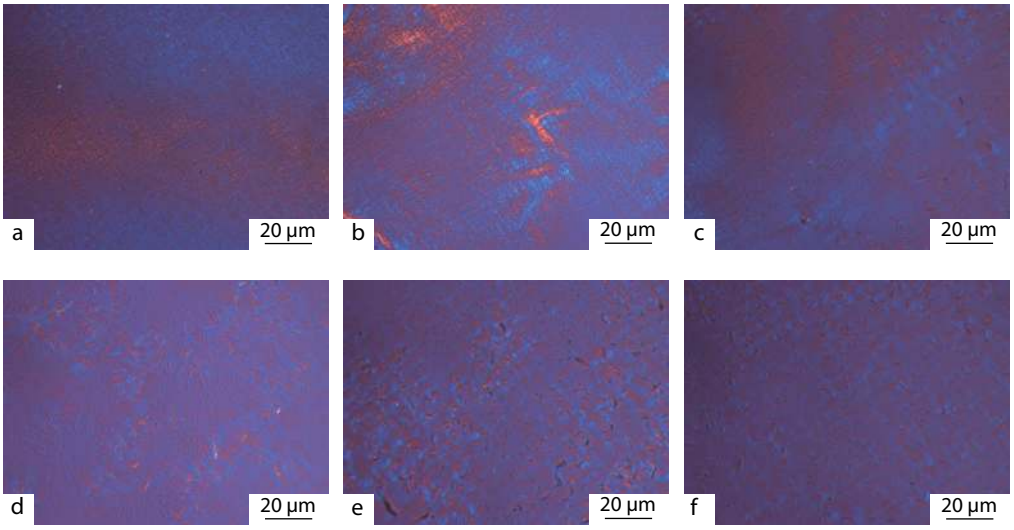

Fig. 4 POM images of (a) HPC, (b) HPC-g_{28}-P(THF$_{104}$-*co*-ECH$_{26}$), (c) HPC-g_{27}-P(THF$_{117}$-*co*-ECH$_{17}$), (d) HPC-g_{24}-P(THF$_{133}$-*co*-ECH$_{11}$), (e) HPC-g_{24}-P(THF$_{177}$-*co*-ECH$_{21}$), and (f) HPC-g_{23}-P(THF$_{201}$-*co*-ECH$_{15}$) graft copolymers.

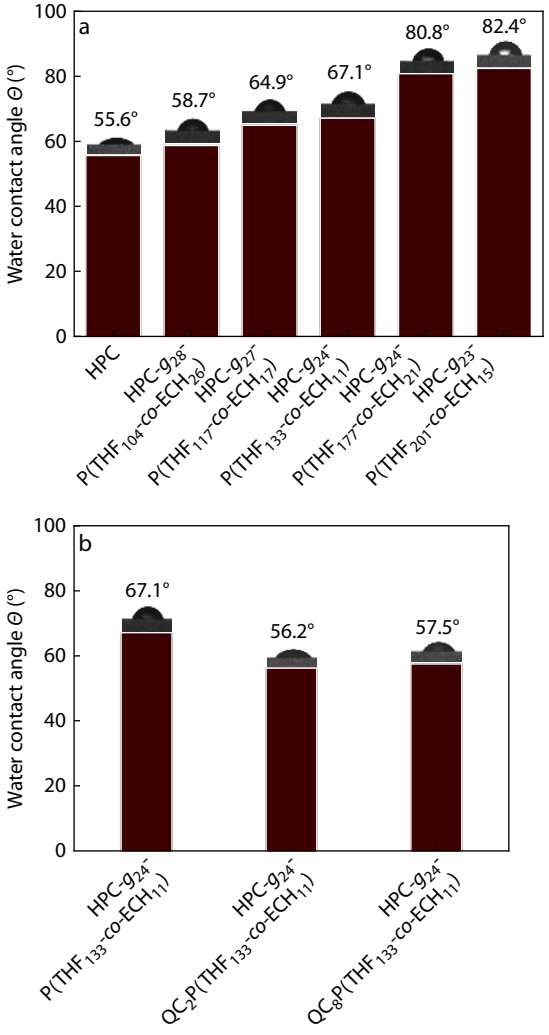

Fig. 5 WCAs on film surfaces of (a) HPC and HPC-*g*-P(THF-*co*-ECH) graft copolymers and (b) HPC-g_{24}-QCP(THF$_{133}$-*co*-ECH$_{11}$) graft copolymers after quaternization.

1209 cm^{-1} is attributed to the C—N bond of the formed quaternary ammonium moiety after quaternization of the graft copolymers. The FTIR characterization preliminarily indicates the successful quaternization of HPC-*g*-P(THF-*co*-ECH) graft copolymers.

The quaternization degree of HPC-*g*-QCP(THF-*co*-ECH) graft copolymer cannot be calculated from integral values of characteristic signals in ^{1}H-NMR spectra since the signals of methylene protons (N$^+$—CH$_2$—) overlap with those of the CH$_2$ and CH protons in AGU. The quaternization degree of HPC-*g*-QCP(THF-*co*-ECH) graft copolymer can be ascertained by XPS characterization according to literature.[41] The XPS spectra of the presentative HPC-g_{24}-P(THF$_{133}$-*co*-ECH$_{11}$) and HPC-g_{24}-QC$_2$P(THF$_{133}$-*co*-ECH$_{11}$) graft copolymers are shown in Fig. 6. The spectra of HPC-*g*-QCP(THF-*co*-ECH) graft copolymers show four main signals corresponding to Cl 2p (200.2 eV), C 1s (285.0 eV), N 1s (400 eV) and O 1s (532 eV) (Fig. 6a). Particularly, there are new peaks in N 1s XPS spectra in Fig. 6(b), and the two peaks at about 399 and 402 eV are attributed to the C—N (from amino) species and C—N$^+$ species (from quaternary ammonium).[41] With respect to HPC-g_{24}-QC$_2$P(THF$_{133}$-*co*-ECH$_{11}$) graft copolymer, its corresponding Cl 2p XPS spectrum (Fig. 6c) shows two peaks at about 201.6 and 200.2 eV, which belong to the C—Cl species (from ECH unit) and —N$^+$Cl$^-$ species (from quaternary ammonium). The quaternization degree was 63.6% for HPC-g_{24}-QC$_2$P(THF$_{133}$-*co*-ECH$_{11}$) graft copolymer determined by the area ratio of —N$^+$Cl$^-$ to (—N$^+$Cl$^-$ + C—Cl). Similarly, the quaternization degree was 58.2% for HPC-g_{24}-QC$_8$P(THF$_{133}$-*co*-ECH$_{11}$) graft copolymer (as shown in Fig. S7 in ESI). The above results indicate that HPC-g_{24}-QC$_2$P(THF$_{133}$-*co*-ECH$_{11}$) and HPC-g_{24}-QC$_8$P(THF$_{133}$-*co*-ECH$_{11}$) graft copolymers could be successfully synthesized and the quaternization degree was determined to be around 60%.

The WCA results of HPC-g_{24}-P(THF$_{133}$-*co*-ECH$_{11}$), HPC-g_{24}-QC$_2$P(THF$_{133}$-*co*-ECH$_{11}$), and HPC-g_{24}-QC$_8$P(THF$_{133}$-*co*-ECH$_{11}$) graft copolymers are given in Fig. 5(b). The WCA decreased by *ca.* 10° after quaternization compared to that of original

https://doi.org/10.1007/s10118-020-2372-3

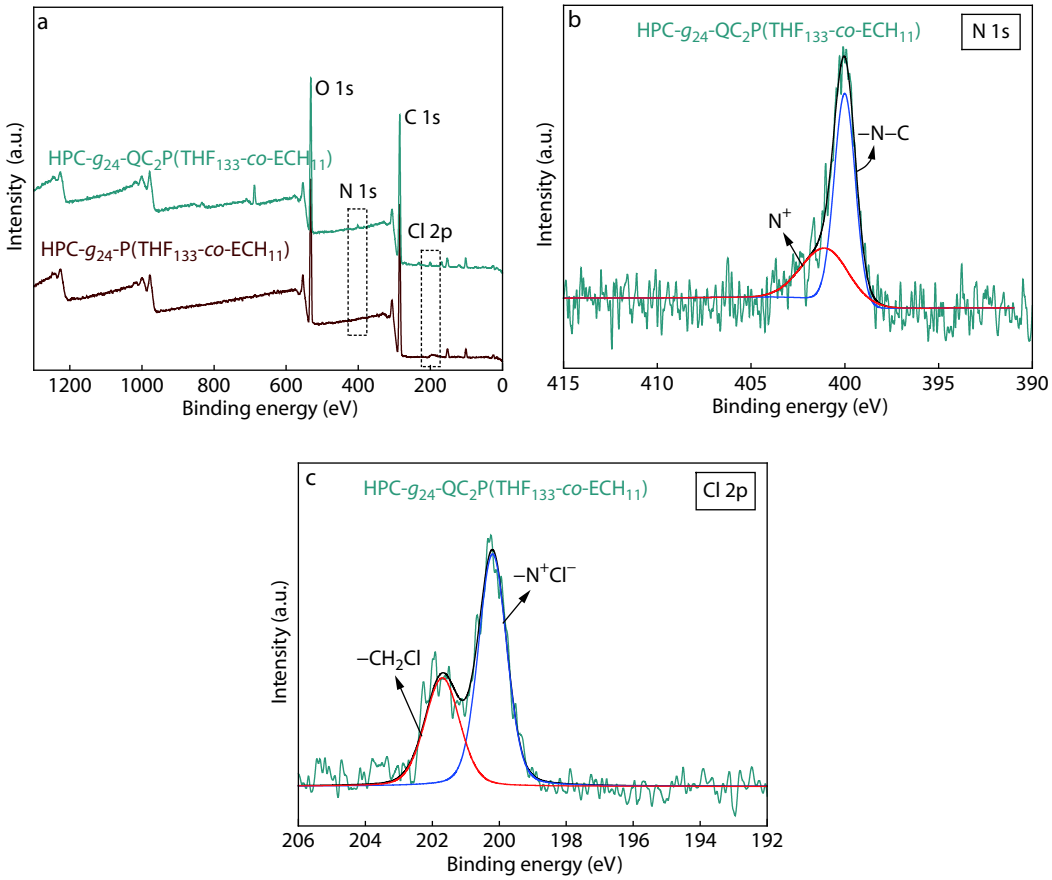

Fig. 6 (a) XPS wide scans of HPC-g_{24}-P(THF$_{133}$-*co*-ECH$_{11}$) and HPC-g_{24}-QC$_2$P(THF$_{133}$-*co*-ECH$_{11}$) graft copolymers; (b) N 1s and (c) Cl 2p spectra of HPC-g_{24}-QC$_2$P(THF$_{133}$-*co*-ECH$_{11}$) graft copolymers.

HPC-g_{24}-P(THF$_{133}$-*co*-ECH$_{11}$) graft copolymer. These results give a further confirmation on the successful quaternization process on HPC-g_{24}-P(THF$_{133}$-*co*-ECH$_{11}$) graft copolymer to synthesize the desired HPC-g_{24}-QC$_2$P(THF$_{133}$-*co*-ECH$_{11}$) and HPC-g_{24}-QC$_8$P(THF$_{133}$-*co*-ECH$_{11}$) graft copolymers.

Antibacterial Properties of HPC-*g*-(QC)P(THF-*co*-ECH) Graft Copolymers

To examine the antibacterial ability of HPC and HPC-*g*-P(THF-*co*-ECH) graft copolymers, drops of HPC and HPC-*g*-P(THF-*co*-ECH) graft copolymers solutions (10 mg/1 mL in distilled water or THF) loaded on the filtering paper (with diameter of 5.5 mm) using 50-μL tip were tested against *E. coli* and *S. aureus* bacteria. The antibacterial ability of HPC and HPC-*g*-P(THF-*co*-ECH) graft copolymers was evaluated by determination of the size of inhibition zone. The better the antibacterial activity, the larger the diameter of inhibition zone. As shown in Fig. 7, an obvious inhibition zone appears in terms of quaternized HPC-g_{24}-QCP(THF$_{133}$-*co*-ECH$_{11}$) graft copolymers due to the —N$^+$R$_3$Cl$^-$ side groups. Interestingly, the HPC-g_{24}-QC$_8$P(THF$_{133}$-*co*-ECH$_{11}$) graft copolymer with a longer alkyl chain demonstrated larger inhibition zones in *E. coli* than that for the HPC-g_{24}-QC$_2$P(THF$_{133}$-*co*-ECH$_{11}$) with a shorter alkyl chain. On the other hand, the HPC-g_{24}-QC$_2$P(THF$_{133}$-*co*-ECH$_{11}$) graft copolymer presented larger inhibition zone for *S. aureu*. It seems that the longer alkyl chains is more effective to *E. coli* and the shorter alkyl chains is more effective to *S. aureus*. These results are in agreement with that in the previous report.[42]

The possible mechanism for antibacterial activity of HPC-g_{24}-QCP(THF$_{133}$-*co*-ECH$_{11}$) graft copolymers might be that the electrostatic interaction between amino groups (with positive charge) and bacteria membranes (with negative charge) results in the destruction of regular live cell structure.

In Vitro Release of IBU from Microparticles of Graft Copolymers

The IBU-loaded microparticles with HPC-g_{24}-P(THF$_{133}$-*co*-ECH$_{11}$) and HPC-g_{24}-QC$_2$P(THF$_{133}$-*co*-ECH$_{11}$) graft copolymer were prepared by using electrospraying (electrohydrodynamic spraying) method. The SEM image and the size-distribution histogram of formed microparticles are presented in Fig. 8. A mean diameter of approximate 3.3 and 3.0 μm with well microparticle size distribution and smooth surface can be seen in the obtained microparticles of HPC-g_{24}-P(THF$_{133}$-*co*-ECH$_{11}$) and HPC-g_{24}-QC$_2$P(THF$_{133}$-*co*-ECH$_{11}$) graft copolymer. Hydrophobic IBU is encapsulated in the HPC-*g*-P(THF-*co*-ECH) graft copolymers with long soft branches through hydrophobic interactions. The drug loading capacity for the above two HPC-*g*-P(THF-*co*-ECH) graft copolymers was slightly different. The drug-loading capacity was 43.7% for HPC-g_{24}-P(THF$_{133}$-*co*-ECH$_{11}$) graft copolymer microparticles and 45.2% for HPC-g_{24}-QC$_2$P(THF$_{133}$-*co*-ECH$_{11}$) graft copolymer microparticles, which is relatively closed to the theoretical value of IBU loading by setting at 50%.

https://doi.org/10.1007/s10118-020-2372-3

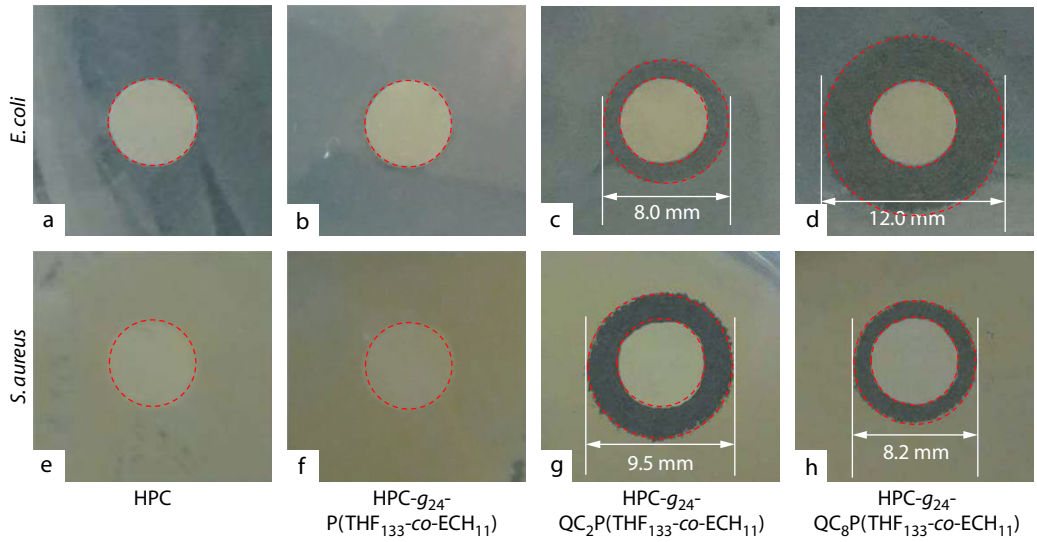

Fig. 7 Photoscopic images of antibacterial activities against (a–d) *E. coli* and (e–h) *S. aureus* on the HPC and HPC-*g*-(QC)P(THF-*co*-ECH) graft copolymers.

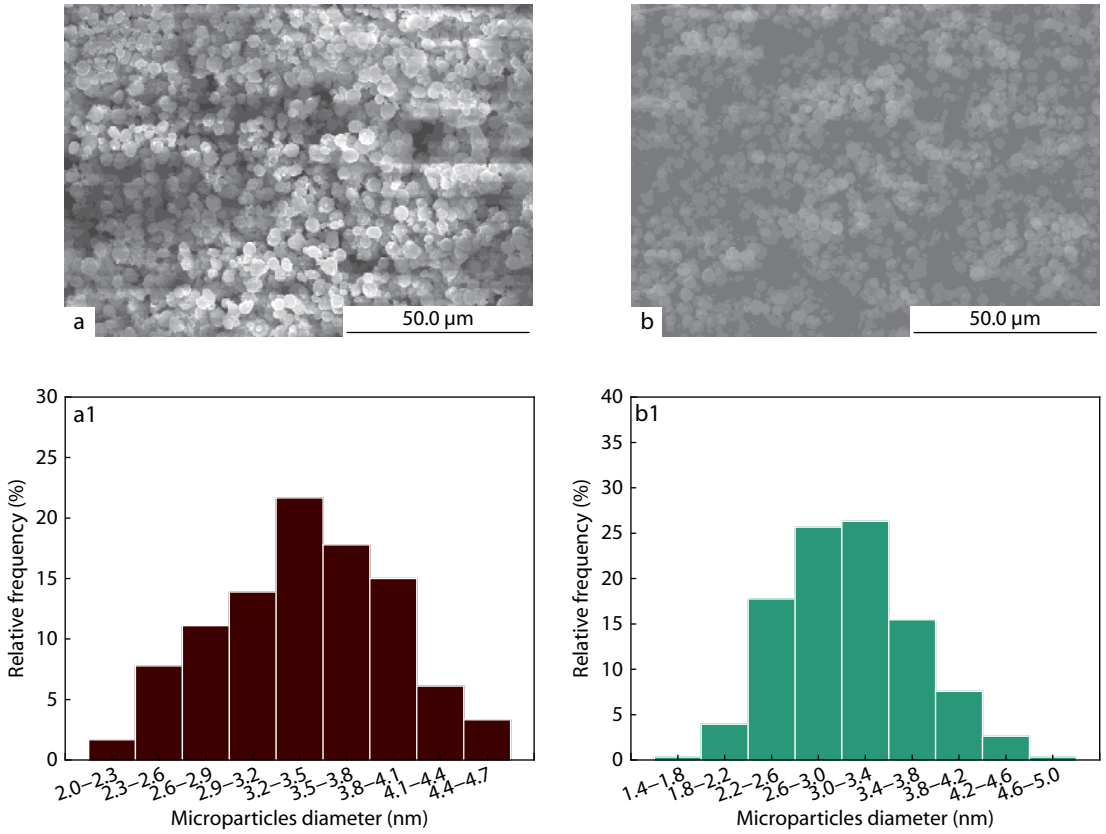

Fig. 8 SEM images of graft copolymer IBU-loaded microparticles of (a) HPC-g_{24}-P(THF$_{133}$-*co*-ECH$_{11}$) and (b) HPC-g_{24}-QC$_2$P(THF$_{133}$-*co*-ECH$_{11}$). Size-distribution histogram of the prepared graft copolymer IBU-loaded microparticles of (a1) HPC-g_{24}-P(THF$_{133}$-*co*-ECH$_{11}$) and (b1) HPC-g_{24}-QC$_2$P(THF$_{133}$-*co*-ECH$_{11}$), as evaluated from 200 measurements.

The *in vitro* drug release performance of IBU-loaded microparticles with HPC-*g*-(QC)P(THF-*co*-ECH) graft copolymer was studied in pH = 1.2 simulated gastric fluid (SGF), pH = 5.0 (tumor acidic microenvironment), pH = 7.4 simulated intestinal fluid (SIF) and pH = 10.0 (a typical basic condition) at 37 °C. Drug release profiles for HPC-g_{24}-P(THF$_{133}$-*co*-ECH$_{11}$) and HPC-g_{24}-QC$_2$P(THF$_{133}$-*co*-ECH$_{11}$) graft copolymer drug carriers in PBS at three pH values are shown in Fig. 9. For the IBU-loaded microparticles with HPC-g_{24}-P(THF$_{133}$-*co*-ECH$_{11}$) graft copolymer, there was no obvious difference in PBS at

https://doi.org/10.1007/s10118-020-2372-3

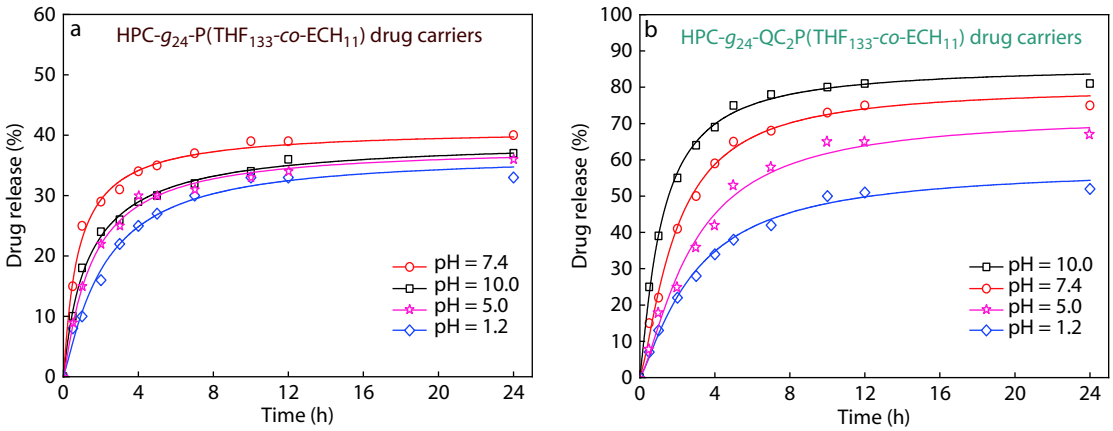

Fig. 9 IBU release profiles of (a) HPC-g_{24}-P(THF$_{133}$-*co*-ECH$_{11}$) and (b) HPC-g_{24}-QC$_2$P(THF$_{133}$-*co*-ECH$_{11}$) graft copolymer IBU-loaded microparticles in PBS at pH = 1.2, 5.0, 7.4 and 10.0 at 37 °C.

four pH values from 1.2 to 10.0 (Fig. 9a), since there are not pH-responsive groups such as carboxyl group and amino group in the HPC-g_{24}-P(THF$_{133}$-*co*-ECH$_{11}$) graft copolymer for further charge dissociation. On the other hand, strong surface-effect between hydrophobic IBU drug and hydrophobic branches occurred in HPC-g_{24}-P(THF$_{133}$-*co*-ECH$_{11}$) graft copolymer. However, IBU-loaded microparticles with HPC-g_{24}-QC$_2$P(THF$_{133}$-*co*-ECH$_{11}$) graft copolymer exhibit the pH-sensitive drug release behavior. In strong acidic conditions of pH = 1.2, a slow release profile was obtained for the IBU encapsulated in microparticles, with about 50.0% IBU release within 8 h and about 52% after 24 h. In a weak acidic conditions of pH = 5.0, about 66% IBU was released after 24 h. At pH = 7.4, about 75% of the IBU was released after 24 h. The release rate of IBU was greatly accelerated under the simulated intestinal conditions. These pH-sensitive drug release behaviors may be mainly attributed to the ionization of quaternary ammonium group in branches of HPC-g_{24}-QC$_2$P(THF$_{133}$-*co*-ECH$_{11}$) graft copolymer at pH = 7.4 and further the branches were dissociated to release the encapsulated IBU. Besides, IBU possesses better solubility in simulated intestinal fluid (SIF), as reported earlier.[43] However, the release rate of IBU was about 80% IBU release within 8 h and about 81% after 24 h under the typical basic condition at pH = 10.0, which might be caused by the ionization of the carboxyl groups.

CONCLUSIONS

We have successfully synthesized novel HPC-*g*-QCP(THF-*co*-ECH) graft copolymers to combine the properties from hydrophilic hard HPC biomacromolecular backbone, hydrophobic flexible polyether branches and functional groups through three steps. The living P(THF-*co*-ECH) chains with chlorine-functional groups were synthesized *via* living CROP of THF with ECH using MeOTf as the initiator at 25 °C. The ECH content in the living P(THF-*co*-ECH) chains could be mediated from 6.9 mol% to 19.7 mol% with M_n in a range from 8900 g·mol^{-1} to 2.66 × 10^4 g·mol^{-1}. DSC result of the P(THF-*co*-ECH) copolymers shows that the melting point of P(THF-*co*-ECH) decreased from 23.9 °C to 15.6 °C with increasing ECH content from 6.9 mol% to 19.7 mol% ECH. The obvious crystalline morphology of HPC-*g*-P(THF-*co*-ECH) graft copolymers mainly depended on the HPC main chains for the HPC-*g*-P(THF-*co*-ECH) graft copolymers with the short branch length. And the band-like structure crystalline morphology is mainly dependent on the polyether branches for the HPC-*g*-P(THF-*co*-ECH) graft copolymers with the long branch length. WCA on thin films of the HPC-*g*-P(THF-*co*-ECH) graft copolymer can be tuned in a range from 58° to 82° and WCA decreased by *ca.* 10° after quaternization. The quaternized HPC-g_{24}-QCP(THF$_{133}$-*co*-ECH$_{11}$) graft copolymers exhibit antibacterial ability against *S. aureus* or *E. coli* bacteria. The ibuprofen (IBU)-loaded microparticles with HPC-*g*-(QC)P(THF-*co*-ECH) graft copolymers were prepared. The IBU release behavior *in vitro* was pH-responsive and up to 75% of drug-loaded could be released at pH = 7.4 in simulated intestinal fluid (SIF) smoothly. These new polyether-grafted cellulosic materials might be potentially used in the fields of antibacterial materials and drug delivery systems.

Electronic Supplementary Information

Electronic supplementary information (ESI) is available free of charge in the online version of this article at https://doi.org/10.1007/s10118-020-2372-3.

ACKNOWLEDGMENTS

This work was financially supported by the National Natural Science Foundation of China (Nos. 21574007 and 51521062).

REFERENCES

1 Herzberger, J.; Niederer, K.; Pohlit, H.; Seiwert, J.; Worm, M.; Wurm, F. R.; Frey, H. Polymerization of ethylene oxide, propylene oxide, and other alkylene oxides: synthesis, novel polymer architectures, and bioconjugation. *Chem. Rev.* **2016**, *116*, 2170–2243.

2 Kobayashi, S.; Danda, H.; Saegusa, T. Superacids and their derivatives IV. Kinetic studies on the ring-opening polymerization of tetrahydrofuran initiated with ethyl trifluoromethanesulfonate by means of ^{19}F and ^{1}H nuclear

magnetic resonance spectroscopy. evidence for the oxonium-ester equilibrium of the propagating species. *Macromolecules* **1974**, *7*, 415–420.
3 Doran, S.; Yilmaz, G.; Yagci, Y. Tandem photoinduced cationic polymerization and CuAAC for macromolecular synthesis. *Macromolecules* **2015**, *48*, 7446–7452.
4 You, L.; Ling, J. Janus polymerization. *Macromolecules* **2014**, *47*, 2219–2225.
5 Lai, Y.; Kuang, X.; Zhu, P.; Huang, M.; Dong, X.; Wang, D. Colorless, transparent, robust, and fast scratch-self-healing elastomers *via* a phase-locked dynamic bonds design. *Adv. Mater.* **2018**, *30*, 1802556.
6 Mi, H. Y.; Jing, X.; Napiwocki, B. N.; Hagerty, B. S.; Chen, G.; Turng, L. S. Biocompatible, degradable thermoplastic polyurethane based on polycaprolactone-block-polytetrahydrofuran-block-polycaprolactone copolymers for soft tissue engineering. *J. Mater. Chem. B* **2017**, *5*, 4137–4151.
7 Kim, D.; Lee, D. G.; Kim, J. C.; Lim, C. S.; Kong, N. S.; Kim, J. H.; Jung, H. W.; Noh, S. M.; Park, Y. I. Effect of molecular weight of polyurethane toughening agent on adhesive strength and rheological characteristics of automotive structural adhesives. *Int. J. Adhes. Adhes.* **2017**, *74*, 21–27.
8 Zhao, J. C.; Du, F. P.; Zhou, X. P.; Cui, W.; Wang, X. M.; Zhu, H.; Xie, X. L.; Mai, Y. W. Thermal conductive and electrical properties of polyurethane/hyperbranched poly(urea-urethane)-grafted multi-walled carbon nanotube composites. *Compos. Part B* **2011**, *42*, 2111–2116.
9 Mu, C. G.; Fan, X. D.; Tian, W.; Bai, Y.; Yang, Z.; Fan, W. W.; Chen, H. Synthesis and stimulus-responsive micellization of a well-defined H-shaped terpolymer. *Polym. Chem.* **2012**, *3*, 3330–3339.
10 Bazban-Shotorbani, S.; Hasani-Sadrabadi, M. M.; Karkhaneh, A.; Serpooshan, V.; Jacob, K. I.; Moshaverinia, A.; Mahmoudi, M. Revisiting structure-property relationship of pH-responsive polymers for drug delivery applications. *J. Control. Release* **2017**, *253*, 46–63.
11 Matricardi, P.; Meo, C. D.; Coviello, T.; Hennink, W. E.; Alhaique, F. Interpenetrating polymer networks polysaccharide hydrogels for drug delivery and tissue engineering. *Adv. Drug Deliver. Rev.* **2013**, *65*, 1172–1187.
12 B.; Thomas, Raj, M. C.; B, A. K.; H, R. M.; Joy, J.; Moores, A.; Drisko, G. L.; Sanchez, C. Nanocellulose, a versatile green platform: from biosources to materials and their applications. *Chem. Rev.* **2018**, *118*, 11575–11625.
13 Xu, F. J.; Zhu, Y.; Liu, F. S.; Nie, J.; Ma, J.; Yang, W. T. Comb-shaped conjugates comprising hydroxypropyl cellulose backbones and low-molecular-weight poly(*N*-isopropylacryamide) side chains for smart hydrogels: synthesis, characterization, and biomedical applications. *Bioconjugate Chem.* **2010**, *21*, 456–464.
14 Chang, C.; Zhang, L. Cellulose-based hydrogels: present status and application prospects. *Carbohydr. Polym.* **2011**, *84*, 40–53.
15 Xu, F. J.; Ping, Y.; Ma, J.; Tang, G. P.; Yang, W. T.; Li, J.; Kang, E. T.; Neoh, K. G. Comb-shaped copolymers composed of hydroxypropyl cellulose backbones and cationic poly((2-dimethyl amino)ethyl methacrylate) side chains for gene delivery. *Bioconjugate Chem.* **2009**, *20*, 1449–1458.
16 Stamatialis, D. F.; Rolevink, H. H. M.; Gironès, M.; Nymeijer, D. C.; Koops, G. H. *In vitro* evaluation of a hydroxypropyl cellulose gel system for transdermal delivery of timolol. *Curr. Drug Deliver.* **2004**, *1*, 313–319.
17 Joubert, F.; Musa, O. M.; Hodgson, D. R. W.; Cameron, N. R. The preparation of graft copolymers of cellulose and cellulose derivatives using ATRP under homogeneous reaction conditions. *Chem. Soc. Rev.* **2014**, *43*, 7217–7235.
18 Tizzotti, M.; Charlot, A.; Fleury, E.; Stenzel, M.; Bernard, J. Modification of polysaccharides through controlled/living radical polymerization grafting-towards the generation of high performance hybrids. *Macromol. Rapid Commun.* **2010**, *31*, 1751–1772.
19 Kang, H.; Liu, R.; Huang, Y. Graft modification of cellulose: methods, properties and applications. *Polymer* **2015**, *70*, A1–A16.
20 Hansson, S.; Trouillet, V.; Tischer, T.; Goldmann, A. S.; Carlmark, A.; Barner-Kowollik, C.; Malmström, E. Grafting efficiency of synthetic polymers onto biomaterials: a comparative study of grafting-from versus grafting-to. *Biomacromolecules* **2013**, *14*, 64–74.
21 Yoo, Y.; Youngblood, J. P. Green one-pot synthesis of surface hydrophobized cellulose nanocrystals in aqueous medium. *ACS Sustain. Chem. Eng.* **2016**, *4*, 3927–3938.
22 Yang, X.; Liu, G.; Peng, L.; Guo, J.; Tao, L.; Yuan, J.; Chang, C.; Wei, Y.; Zhang, L. Highly efficient self-healable and dual responsive cellulose-based hydrogels for controlled release and 3D cell culture. *Adv. Funct. Mater.* **2017**, *27*, 1703174.
23 Liu, Z.; Chen, M.; Guo, Y,; Wang, X.; Zhang, L.; Zhou, J.; Li, H.; Shi, Q. Self-assembly of cationic amphiphilic cellulose-*g*-poly(*p*-dioxanone) copolymers. *Carbohydr. Polym.* **2019**, *204*, 214–222.
24 Cheng, M.; He, H.; Zhu, H.; Guo, W.; Chen, W.; Xue, F.; Zhou, S.; Chen, X.; Wang, S. Preparation and properties of pH-responsive reversible-wettability biomass cellulose-based material for controllable oil/water separation. *Carbohydr. Polym.* **2019**, *203*, 246–255.
25 Li, B.; Zhang, Y.; Wu, C.; Guo, B.; Luo, Z. Fabrication of mechanically tough and self-recoverable nanocomposite hydrogels from polyacrylamide grafted cellulose nanocrystal and poly(acrylic acid). *Carbohydr. Polym.* **2018**, *198*, 1–8.
26 Bai, C.; Huang, X.; Xie, F.; Xiong, X. Microcrystalline cellulose surface-modified with acrylamide for reinforcement of hydrogels. *ACS Sustain. Chem. Eng.* **2018**, *6*, 12320–12327.
27 Esmaeili, A.; Haseli, M. Optimization, synthesis, and characterization of coaxial electrospun sodium carboxymethyl cellulose-graft-methyl acrylate/poly(ethylene oxide) nanofibers for potential drug-delivery applications. *Carbohydr. Polym.* **2017**, *173*, 645–653.
28 Rajesh, S.; Crandall, C.; Schneiderman, S.; Menkhaus, T. J. Cellulose-graft-polyethyleneamidoamine anion-exchange nanofiber membranes for simultaneous protein adsorption and virus filtration. *ACS Appl. Nano Mater.* **2018**, *1*, 3321–3330.
29 Demircan, D.; Zhang, B. Facile synthesis of novel soluble cellulose-grafted hyperbranchedpolymers as potential natural antimicrobial materials. *Carbohydr. Polym.* **2017**, *157*, 1913–1921.
30 Zhao, J.; Li, Q.; Zhang, X.; Xiao, M.; Zhang, W.; Lu, C. Grafting of polyethylenimine onto cellulose nanofibers for interfacial enhancement in their epoxy nanocomposites. *Carbohydr. Polym.* **2017**, *157*, 1419–1425.
31 Li, M.; Gong, Y.; Wang, W.; Xu, G.; Liu, Y.; Guo, J. *In-situ* reduced silver nanoparticles on populus fiber and the catalytic application. *Appl. Surf. Sci.* **2017**, *394*, 351–357.
32 Ma, P.; Shen, T.; Lin, L.; Dong, W.; Chen, M. Cellulose-*g*-poly(D-lactide) nanohybrids induced significant low melt viscosity and fast crystallization of fully bio-based nanocomposites. *Carbohydr. Polym.* **2017**, *155*, 498–506.
33 Ci, J.; Kang, H.; Liu, C.; He, A.; Liu, R. Thermal sensitivity and protein anti-adsorption of hydroxypropyl cellulose-*g*-poly(2-(methacryloyloxy) ethyl phosphorylcholine). *Carbohydr. Polym.* **2017**, *157*, 757–765.
34 Ott, M. W.; Herbert, H.; Graf, M.; Biesalski, M. Cellulose-graft-

polystyrene bottle-brush copolymers by homogeneous RAFT polymerization of soluble cellulose macro-CTAs and "CTA-shuttled" R-group approach. *Polymer* **2016**, *98*, 505–515.
35 Yuan, H.; Chi, H.; Yuan, W. Ethyl cellulose amphiphilic graft copolymers with lcst-ucst transition: opposite self-assembly behavior, hydrophilic-hydrophobic surface and tunable crystalline morphologies. *Carbohydr. Polym.* **2016**, *147*, 261–271.
36 Kalaoğlu, Ö. İ.; Ünlü, C. H.; Galioğlu Atıcı, O. Synthesis, characterization and electrospinning of corn cob cellulose-*graft*-polyacrylonitrile and their clay nanocomposites. *Carbohydr. Polym.* **2016**, *147*, 37–44.
37 Guo, A.; Yang, F.; Yu, R.; Wu, Y. Real-time monitoring of living cationic ring-opening polymerization of THF and direct prediction of equilibrium molecular weight of polyTHF. *Chinese J. Polym. Sci.* **2015**, *33*, 23–35.
38 Guo, A.; Yang, W.; Yang, F.; Yu, R.; Wu, Y. Well-defined poly(γ-benzyl-L-glutamate)-*g*-polytetrahydrofuran: synthesis, characterization, and properties. *Macromolecules* **2014**, *47*, 5450–5461.
39 Wei, M.; Guo, A.; Wu, Y. Microstructure and micromorphology of poly(γ-benzyl-L-glutamate)-*g*-(polytetrahydrofuran-*b*-polyisobutylene) copolymer. *Acta Polymerica Sinica* (in Chinese) **2017**, 506–515.
40 Chang, T.; Zhang, H.; Lu, C.; Wu, Y. *In situ* synthesis and characterization of chitosan-*g*-polytetrahydrofuran graft copolymer/Ag nanocomposite *via* living cationic polymerization. *Acta Polymerica Sinica* (in Chinese) **2018**, 700–711.
41 Yao, C.; Li, X.; Neoh, K. G.; Shi, Z.; Kang, E. T. Surface modification and antibacterial activity of electrospun polyurethane fibrous membranes with quaternary ammonium moieties. *J. Membr. Sci.* **2008**, *320*, 259–267.
42 Zhu, Y.; Xu, C.; Zhang, N.; Ding, X.; Yu, B.; Xu, F. J. Polycationic synergistic antibacterial agents with multiple functional components for efficient anti-infective therapy. *Adv. Funct. Mater.* **2018**, *28*, 1706709.
43 Hadgraft, J.; Valenta, C. pH, pK_a and dermal delivery. *Int. J. Pharm.* **2000**, *200*, 243–247.

https://doi.org/10.1007/s10118-020-2372-3